# Probing the Locality of Excited States with Linear Algebra

Thibaud Etienne*

CNRS, Théorie-Modélisation-Simulation, SRSMC, , Université de Lorraine—Nancy, Boulevard des Aiguillettes 54506, Vandoeuvre-lès-Nancy, France

Unité de Chimie Physique Théorique et Structurale, Université de Namur, Rue de Bruxelles 61, 5000 Namur, Belgium

ABSTRACT: This article reports a novel theoretical approach related to the analysis of molecular excited states. The strategy introduced here involves gathering two pieces of physical information, coming from Hilbert and direct space operations, into a general, unique quantum mechanical descriptor of electronic transitions' locality. Moreover, the projection of Hilbert and direct space-derived indices in an Argand plane delivers a straightforward way to visually probe the ability of a dye to undergo a long- or short-range charge-transfer. This information can be applied, for instance, to the analysis of the electronic response of families of dyes to light absorption by unveiling the trend of a given push–pull chromophore to increase the electronic cloud polarization magnitude of its main transition with respect to the size extension of its conjugated spacer. We finally demonstrate that all the quantities reported in this article can be reliably approximated by a linear algebraic derivation, based on the contraction of detachment/attachment density matrices from canonical to atomic space. This alternative derivation has the remarkable advantage of a very low computational cost with respect to the previously used numerical integrations, making fast and accurate characterization of large molecular systems' excited states easily affordable.
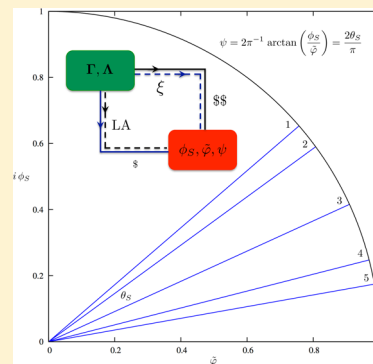
1. INTRODUCTION

Unraveling the physical nature of excited states with quantum chemistry is a challenge that has recently received considerable interest from the theoretical community in molecular physics. To this end, various qualitative[1−10] and quantitative[11−23] approaches have been introduced to tackle real-life chemical issues. Those approaches were already shown to be of high interest for handling public health,[24,25] environmental,[26−32] and military[33,34] stakes, for instance. They often involve a rigorous rationalization of electronic transitions' topological analysis. Since a large variety of crucial applications can benefit from these fundamental developments, their utility paved the way toward the elaboration of novel accurate theoretical methods designed for analysis of excited states. Indeed, general, straightforward, and cost-effective strategies are especially targeted.

Preliminary investigations already reported various possible computational strategies, including exciton wave function analysis[11−14] and evaluation of particle−hole densities overlap[14,15] or inter-centroid distances,[15−23] for example. It was also shown that, despite their complementarity, some of these approaches can suffer some limitations due to geometrical considerations related to molecular symmetry.[15] Nevertheless, these methodologies can be shown to be compatible, as they consistently provide different insightful information with regard to the topology of excited states.[15] In this article, we shed light on this compatibility and use it to elaborate a more general tool for describing the electronic structure reorganization occurring upon light absorption. Indeed, two of the previously extensively validated topological indices arising from Hilbert and direct space operations followed by numerical integration, respectively

the overlap ϕ_S and the charge transfer $\tilde{\chi}$ integrals, will be used to build a unique descriptor, ψ, that exploits the different origins of its two components for gathering physical information arising from two types of operations involving density matrices and electron density.

This novel general descriptor's use is illustrated with a model compound. We further show the interest of projecting ψ in the Argand plane by considering a family of dyes (five oligomers derived from 1,4-nitroaniline) to highlight the π-spacer's influence on the ψ index value.

Afterward, we report an alternative derivation of the key quantities discussed herein. This second derivation involves only highly cost-effective linear algebraic operations and is proved to give a reliable approximation of our topological indices. In the case of large molecules, this strategy is shown to be an efficient substitute for the numerical integrations previously in use.

Finally, a global discussion of the efficiency/accuracy ratio of four possible derivations of the ϕ_S, $\tilde{\chi}$, and ψ indices (i.e., combinations of ground/excited states or transition density matrices analysis with numerical integration or linear algebra) is delivered.

2. THEORETICAL BACKGROUND AND COMPUTATIONAL DETAILS

This section aims at providing the primary tools required for the formal construction of the ϕ_S and $\tilde{\chi}$ (section 2.1) descriptors, the ψ (section 2.2) index, and their assessment

$$(\boldsymbol{\sigma}_\pm)_{kj} = \frac{1}{2}\left(\sqrt{(\boldsymbol{\delta})_{kk}^2} \pm (\boldsymbol{\delta})_{kk}\right) \times \delta_{kj} \mid \boldsymbol{\delta} = \sum_{\omega=+,-} \omega\, \boldsymbol{\sigma}_\omega$$
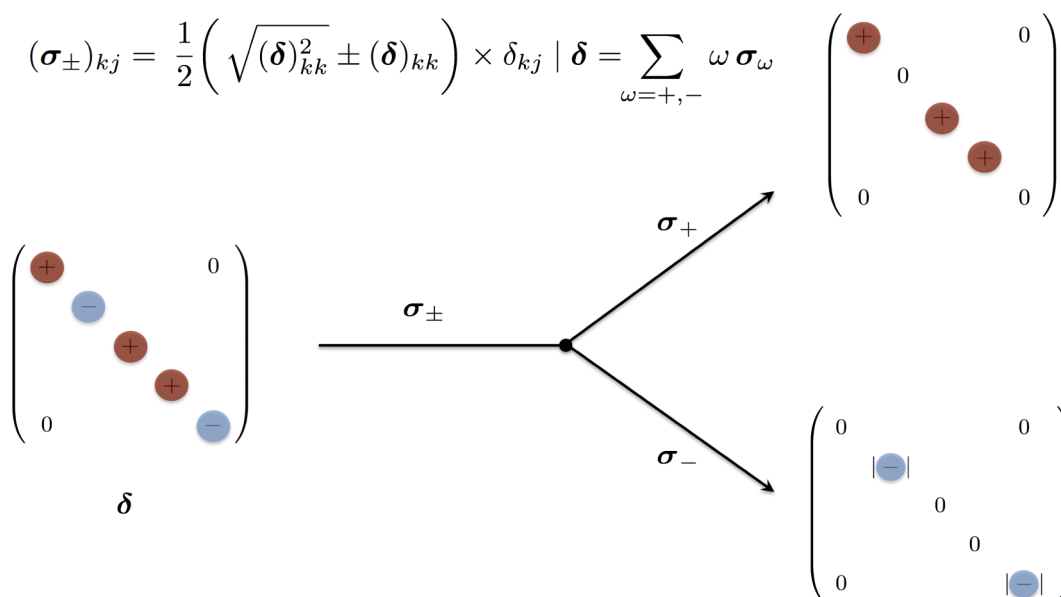
Figure 1. Illustration of the $\boldsymbol{\delta}$ matrix splitting with respect to the $\boldsymbol{\Delta}$ eigenvalues signs.
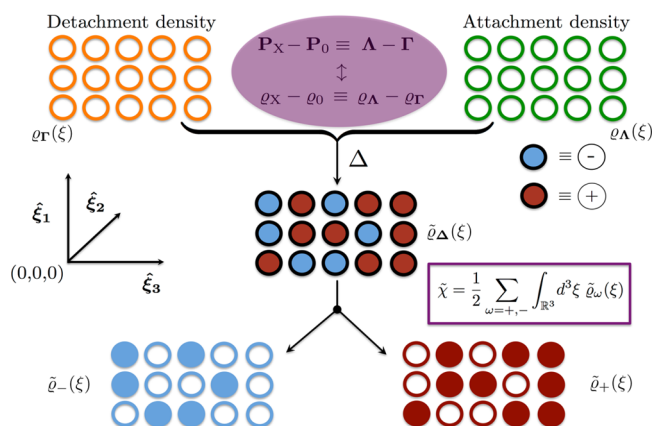

Figure 2. Graphical illustration of the obtention of $\tilde{\chi}$ from detachment/attachment densities in real space.

through linear algebra calculations (section 2.3). It further gives details about the computations performed throughout this paper (section 2.4). For more information about the ϕ_S and $\tilde{\chi}$ indices, we invite the reader to consult refs 14 and 15.

2.1. Hilbert and Direct Space Derivation of Two Topological Descriptors, ϕ_S and $\tilde{\chi}$. The ϕ_S and $\tilde{\chi}$ indices are charge-transfer metrics related to the electronic cloud polarization in a complementary way. Indeed, if one pictures an electronic transition phenomenon as an electron−hole generation, it is possible to use the exciton wave function or the ground-state/excited-state density matrices to locate the depletion (detachment) and increment (attachment) zones of electron density. Some basic operations can further lead to a quantitative assessment of the charge-transfer character of the target transition. One can, for instance, consider the spatial overlap between the hole and the particle densities, which constitutes the ϕ_S integral. Another possible quantitative way to probe the locality of excited states involves computing the fraction of charge that has been displaced during the transition, which corresponds to the charge-transfer integral $\tilde{\chi}$. Both descriptors bear different but complementary physical information derived from a splitting operation (see Figure 1)
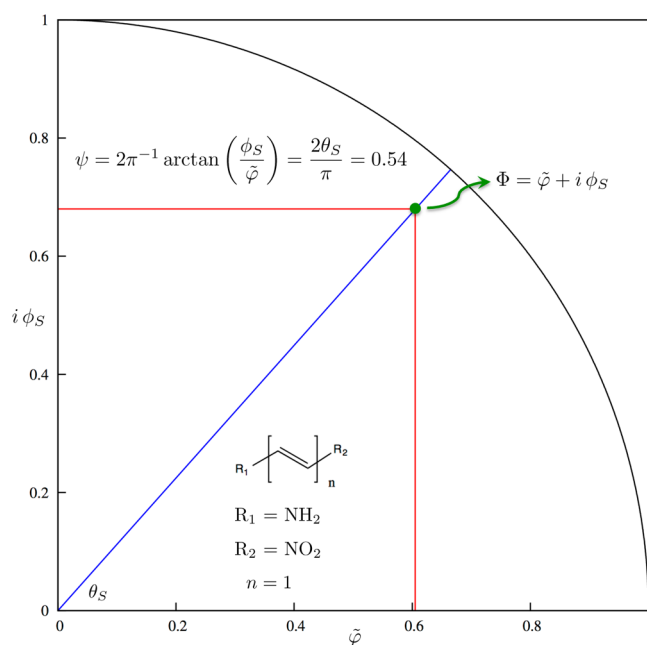

Figure 3. Projection of the Φ number in the Argand plane for a simple push−pull molecule.

performed in Hilbert (ϕ_S) or direct ($\tilde{\chi}$) space. Obviously these metrics are fundamentally connected to each other in the sense that a significant charge displacement will lead to a low overlap between the detachment and attachment densities. The reverse is also true.

One possible way (see the black-arrowed path in Figure 7, below) to derive the ϕ_S and $\tilde{\chi}$ indices requires considering the singular value decomposition[35] of the transition density matrix[36−39] **T** (which couples ground to excited states in the canonical space), i.e., the obtention of the **O** and **V** matrices that may be used for the unitary transformation of **T** into the diagonal matrix **W**, storing the so-called singular values w of **T**:

$$\exists\, \mathbf{O}, \mathbf{V} \mid (\mathbf{O}^\dagger \mathbf{T} \mathbf{V})_{ij} = (\mathbf{W})_{ij} = w_{ij}\delta_{ij} \tag{1}$$

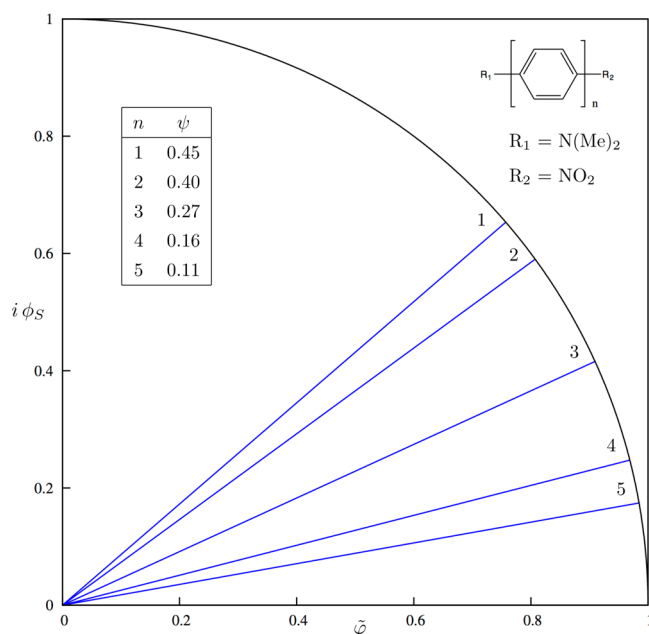| n	ψ
1	0.45
2	0.40
3	0.27
4	0.16
5	0.11

$R_1 = N(Me)_2$
$R_2 = NO_2$

Figure 4. Projection of the ψ number in the Argand plane from the origin to the trigonometric circle for a family of dyes derived from the 1,4-nitroaniline compound.

These **O** and **V** matrices can be used to perform a rotation over the occupied and virtual canonical orbitals, whose linear combination of atomic orbitals (LCAO) coefficients are stored in the $\tilde{\mathbf{O}}$ and $\tilde{\mathbf{V}}$ matrices, respectively. The products of these two rotations are the so-called "occupied" and "virtual" natural transition orbitals (NTOs), whose coefficients are stored in the $\mathbf{C}^o$ and $\mathbf{C}^v$ matrices:

$$\mathbf{C}^o = \tilde{\mathbf{O}}\mathbf{O}, \quad \mathbf{C}^v = \tilde{\mathbf{V}}\mathbf{V} \tag{2}$$

These NTO coefficient matrices can be used together with the squared singular values of **T** to write the occupied and virtual density matrices, $\mathbf{P}^o$ and $\mathbf{P}^v$.

$$(\mathbf{P}^o)_{ij} = \sum_{l=1}^{N_o} w_{ll}^2 (\mathbf{C}^o)_{il}(\mathbf{C}^o)_{jl}, \quad (\mathbf{P}^v)_{ij} = \sum_{l=1}^{N_v} w_{ll}^2 (\mathbf{C}^v)_{il}(\mathbf{C}^v)_{jl} \tag{3}$$

It has previously been shown[15] that, under certain conditions, the difference between excited ($\mathbf{P}_X$) and ground ($\mathbf{P}_0$) states' density matrices is equal to the difference between the virtual and occupied density matrices. The resulting $\mathbf{\Delta}$ matrix can further be diagonalized into $\boldsymbol{\delta}$,

$$\mathbf{P}_X - \mathbf{P}_0 = \mathbf{\Delta} = \mathbf{P}^v - \mathbf{P}^o \quad \Rightarrow \quad \exists \mathbf{U} \mid (\boldsymbol{\delta})_{ij} = (\mathbf{U}^\dagger \mathbf{\Delta} \mathbf{U})_{ij} = 0 \quad \forall i \neq j \tag{4}$$

and a proper treatment of the $\mathbf{\Delta}$ eigenvalues, based on the sign of the $\boldsymbol{\delta}$ entries, returns the $\boldsymbol{\sigma}_\pm$ arrays and allows us to construct two final matrices, $\mathbf{\Gamma}$ and $\mathbf{\Lambda}$, from the back-transformation of $\boldsymbol{\sigma}_-$ and $\boldsymbol{\sigma}_+$, respectively (these operations are illustrated in Figure 1):

$$(\sigma_\pm)_{kj} = \frac{1}{2}\left(\sqrt{(\delta)_{kk}^2} \pm (\delta)_{kk}\right) \times \delta_{kj} \mid \boldsymbol{\delta} = \sum_{\omega=+,-} \omega\, \boldsymbol{\sigma}_\omega \;;$$

$$\mathbf{\Delta} = \mathbf{U}\boldsymbol{\delta}\mathbf{U}^\dagger = \sum_{\omega=+,-} \omega\, \mathbf{U}\boldsymbol{\sigma}_\omega \mathbf{U}^\dagger \equiv \mathbf{\Lambda} - \mathbf{\Gamma} \tag{5}$$

These so-called detachment and attachment density matrices ($\mathbf{\Gamma}$ and $\mathbf{\Lambda}$, respectively) describe in the Hilbert space the depletion and increment of electron density caused by photon

capture. They can equivalently[14] be set from Hilbert space transformations based on the ground and excited states' density matrices (see the blue-arrowed path in Figure 7, below), where the $\mathbf{\Delta}$ matrix is simply taken as the difference between excited and ground states' density matrices—see (4). Actually, this original ground/excited states derivation of the difference density matrix and the quantum-mechanical descriptors in this paragraph is more general than the alternative one involving NTOs, since it uses only ground/excited states' density matrices instead of requiring singular value decomposition of a transition density matrix under certain conditions.

From the direct space transposition of $\mathbf{\Gamma}$ and $\mathbf{\Lambda}$ into $\varrho_\Gamma(\xi)$ and $\varrho_\Lambda(\xi)$, i.e., the projection of detachment and attachment density matrices in the real space, we previously[14] defined a dimensionless overlap integral, ϕ_S, as the normalized overlap between the detachment and attachment densities:

$$\phi_S = \vartheta^{-1} \int_{\mathbb{R}^3} d^3\xi \sqrt{\varrho_\Gamma(\xi)\varrho_\Lambda(\xi)}$$

$$\vartheta \equiv \frac{1}{2}\left[\int_{\mathbb{R}^3} d^3\xi \sum_{\tau=\Gamma,\Lambda} \varrho_\tau(\xi)\right] \qquad \phi_S \in [0; 1] \tag{6}$$

where ξ accounts for the three spatial dimensions (ξ_1, ξ_2, ξ_3). This ϕ_S descriptor has bounded values ranging from 0 to 1, depending on the locality of the target transitions. The lowest bounded value depicts a total charge transfer (no overlap), while a strictly local transition (no electron density displacement) will be characterized by an extreme value of 1 for the ϕ_S index.

We now turn to the evaluation of the second key quantity, $\tilde{\chi}$.[15] For this purpose, we need to evaluate the difference between attachment and detachment densities in the three-dimensional space and to split the obtained function in two distinct ones, as we did in (5):

$$\tilde{\varrho}_\Delta(\xi) = \varrho_\Lambda(\xi) - \varrho_\Gamma(\xi)$$

$$\tilde{\varrho}_\pm(\xi) = \frac{1}{2}\left(\sqrt{\tilde{\varrho}_\Delta^2(\xi)} \pm \tilde{\varrho}_\Delta(\xi)\right) \tag{7}$$

Note that since no electron is gained or lost, we have

$$\sum_{\omega=+,-} \omega \int_{\mathbb{R}^3} d^3\xi \tilde{\varrho}_\omega(\xi) = 0 \tag{8}$$

The $\tilde{\chi}$ index is simply defined as

$$\tilde{\chi}_\omega = \int_{\mathbb{R}^3} d^3\xi \tilde{\varrho}_\omega(\xi)$$

$$\tilde{\chi} = \frac{1}{2}\left[\int_{\mathbb{R}^3} d^3\xi \sum_{\omega=+,-} \tilde{\varrho}_\omega(\xi)\right] = \frac{1}{2}\sum_{\omega=+,-} \tilde{\chi}_\omega \tag{9}$$

and its obtention from $\tilde{\varrho}_\Delta$ and $\tilde{\varrho}_\omega$ is graphically depicted in Figure 2. The relationships highlighted in purple at the top of the figure imply that the $\tilde{\chi}$ index can equivalently be derived by using ground and excited states' densities or detachment/attachment densities. Note that the "~" at the top of the ϱ and χ symbols actually recalls that we are using the detachment/attachment derivation pathway rather than ground/excited states' densities.

2.2. Toward a Unique Topological Descriptor, the ψ Index. In this section, we will see that the $\tilde{\chi}$ index can be normalized into $\tilde{\varphi}$ and used together with ϕ_S to build the general ψ index. From (7), it appears that

$$\forall \xi \mid \varrho_\Lambda(\xi) \geq \varrho_\Gamma(\xi), \; +\tilde{\varrho}_+(\xi) = \tilde{\varrho}_\Delta(\xi) \leq +\varrho_\Lambda(\xi) \tag{10}$$
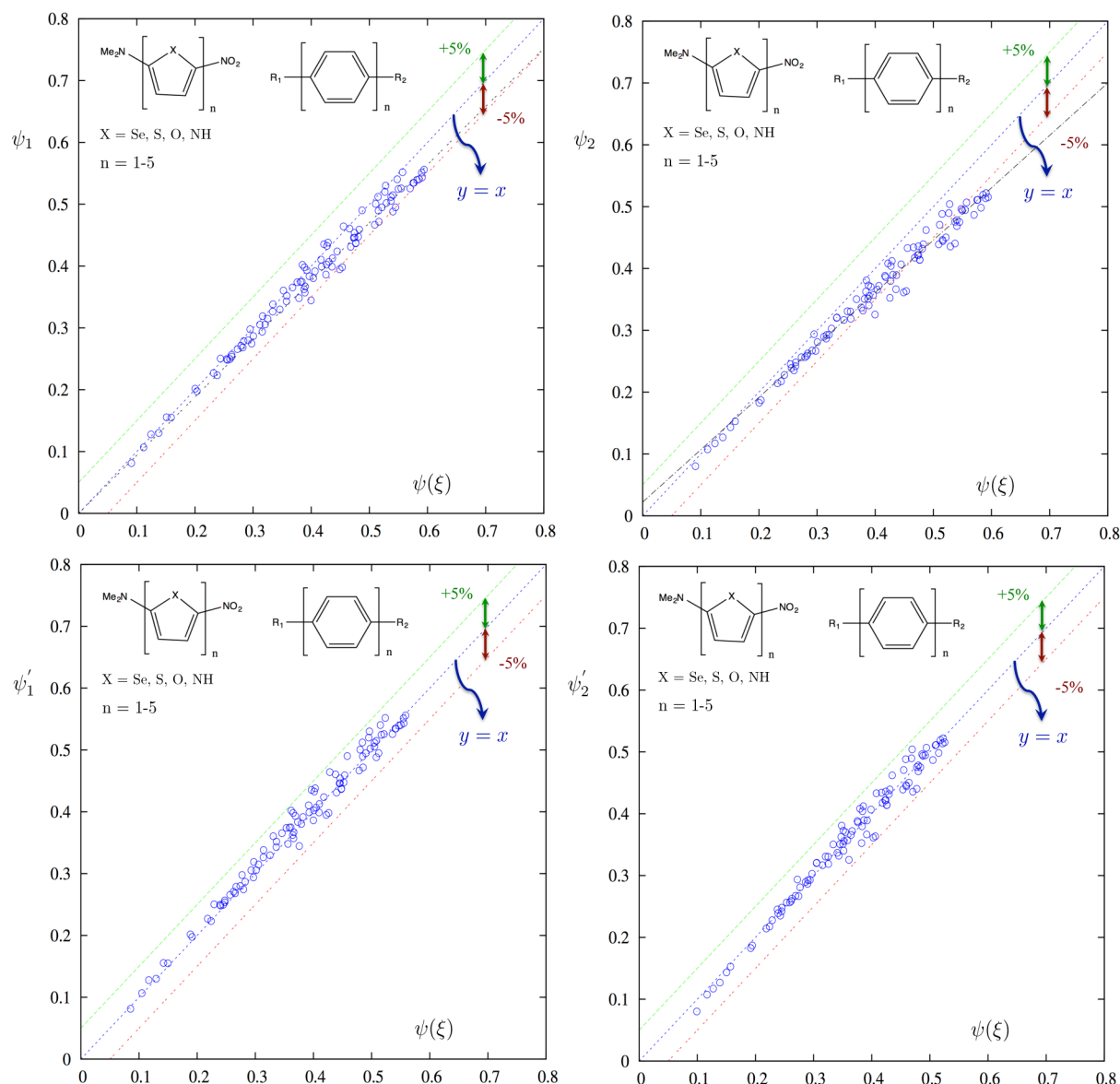
Figure 5. Plot of the linear algebraic vs numerical integration assessment to ψ with η values of 1 (left) and 2 (right), before (top) and after (bottom) linear regression. R^2 values are 0.960 (ψ_1), 0.969 (ψ_1'), 0.861 (ψ_2), and 0.979 (ψ_2').

and

$$\forall \xi \mid \varrho_{\Lambda}(\xi) \leq \varrho_{\Gamma}(\xi) \,,\; -\tilde{\varrho}_{-}(\xi) = \tilde{\varrho}_{\Delta}(\xi) \geq -\varrho_{\Gamma}(\xi) \tag{11}$$

which leads to

$$\tilde{\varrho}_{+}(\xi) \leq \varrho_{\Lambda}(\xi) \;\; \forall \xi \mid \tilde{\varrho}_{\Delta}(\xi) \geq 0 \quad \& $$
$$\tilde{\varrho}_{-}(\xi) \leq \varrho_{\Gamma}(\xi) \;\; \forall \xi \mid \tilde{\varrho}_{\Delta}(\xi) \leq 0 \tag{12}$$

Considering (9) and (12), we can deduce that

$$\tilde{\chi} = \tfrac{1}{2} \sum_{\omega=+,-} \int_{\mathbb{R}^3} \mathrm{d}^3 \xi \, \tilde{\varrho}_{\omega}(\xi) \leq \tfrac{1}{2} \sum_{\tau=\Gamma,\Lambda} \int_{\mathbb{R}^3} \mathrm{d}^3 \xi \, \varrho_{\tau}(\xi) = \vartheta$$
$$\exists! \; \tilde{\varphi} = \vartheta^{-1} \tilde{\chi} \mid \tilde{\varphi} \in [0; 1] \tag{13}$$

We have two normalized descriptors, ϕ_S and $\tilde{\varphi}$. Their definitions arise from different origins: the former is built from Hilbert space transformations performed on occupied (alternatively, ground state) and virtual (excited state) density matrices, followed by a numerical integration in the direct space. The latter is defined by direct space operations followed by a numerical integration. As pointed out in our previous

publication,[15] they deliver significantly different information, but their contributions can be regarded as being complementary. We can therefore define a new complex number, Φ, whose real part is the normalized charge-transfer index $\tilde{\varphi}$, and whose imaginary part is the ϕ_S index value. Φ therefore is written

$$\Phi = \tilde{\varphi} + i\phi_S \Rightarrow 4\frac{\Phi\Phi^*}{(\Phi + \Phi^*)^2} - 1 = \left(\frac{\phi_S}{\tilde{\varphi}}\right)^2 \tag{14}$$

and projects its coordinates in an Argand plane, as we did in Figure 3, where we took a simple push−pull dye as an illustrative example. For the sake of convenience in the projection of Φ in the complex plane, we will refer to the real angle, θ_S:

λ	f	w_{11}^2	w_{22}^2
446	0.2811	0.416	0.414
$\psi(\mathbf{\Delta})$	$\psi_1(\mathbf{\Delta})$	$\psi(\mathbf{T})$	$\psi_1(\mathbf{T})$
0.52	0.51	0.52	0.51

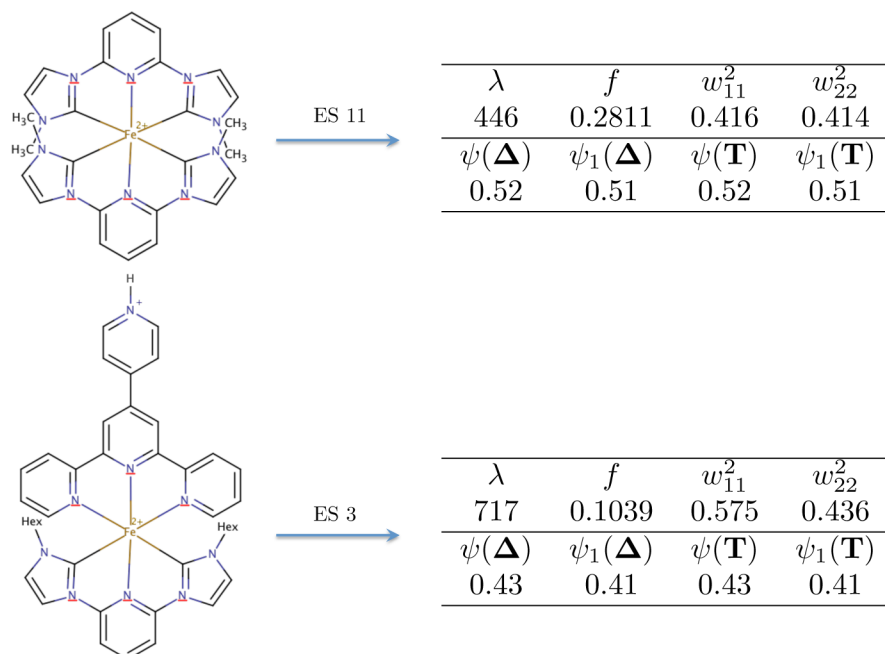| λ	f	w_{11}^2	w_{22}^2
717	0.1039	0.575	0.436
$\psi(\mathbf{\Delta})$	$\psi_1(\mathbf{\Delta})$	$\psi(\mathbf{T})$	$\psi_1(\mathbf{T})$
0.43	0.41	0.43	0.41

Figure 6. (Left) Sketch of the homoleptic (top) and heteroleptic (bottom) iron-based complexes, for which 11th and 3rd transitions are detailed to the right. λ is the transition wavelength (in nm), f is the oscillator strength (in arbitrary units), w^2 entries are the squared singular values corresponding to the NTOs couples 1 (w_{11}^2) and 2 (w_{22}^2). The $\mathbf{\Delta}$ and $\mathbf{T}$ in parentheses designate the ground/excited states' density matrices or transition density matrix derivation of ψ and ψ_1.

$$\theta_S : \mathbb{C} \longrightarrow \mathbb{R}^+$$
$$\Phi \longmapsto \arctan \underbrace{\sqrt{4 \frac{\Phi\Phi^*}{(\Phi + \Phi^*)^2} - 1}}_{\frac{\phi_S}{\tilde{\varphi}}} \qquad \theta_S \in \left[0 ; \frac{\pi}{2}\right[\qquad (15)$$

θ_S is the angle formed between the abscissa axis (i.e., the real axis) and the projection of Φ from the origin to the trigonometric circle. Its values are bounded to 0 and $\pi/2$, so we can write our ultimate unique descriptor ψ as

$$\psi : \mathbb{R}_1^+ \times \mathbb{R}_0^+ \longrightarrow \mathbb{R}_1^+$$
$$(\phi_S, \tilde{\varphi}) \longmapsto 2\pi^{-1} \underbrace{\arctan\left(\frac{\phi_S}{\tilde{\varphi}}\right)}_{\theta_S} \equiv \frac{2\theta_S}{\pi} \quad \psi \in [0 ; 1[\quad (16)$$

so that the ψ descriptor is the normalization of θ_S. Note that, in the previous notation, $\mathbb{R}_x^+$ stands for the positive real ensemble from which x was excluded ($\mathbb{R}^+\backslash\{x\}$). In order to prevent singularities in the ψ function, we excluded from its domain the values for ϕ_S and $\tilde{\chi}$ that would depict the non-physical case where photon capture provokes strictly zero electron-density displacement.

2.3. Linear Algebraic Derivation of ϕ_S, $\tilde{\varphi}$, and ψ. For a K-sized atomic orbitals basis set, the overlap matrix ($\mathbf{S}$) is $K \times K$-sized. We can define two new sets of functions, $\{\eta = 1 \mid \gamma_1, \lambda_1\}$ and $\{\eta = 2 \mid \gamma_2, \lambda_2\}$, as described in (17). Note that, in the following, $\eta = 1$ can be regarded as a Löwdin-like detachment/attachment population analysis, while $\eta = 2$ denotes a Mulliken-like approach. For the sake of brevity, we will keep a single compact nomenclature throughout this paragraph, so that if η is replaced by either 1 or 2, the physical meaning of the approach will match one of the two analyses.

$$\left.\begin{array}{l} \gamma_\eta(k) = (\mathbf{S}^x \mathbf{\Gamma} \mathbf{S}^y)_{kk} \\ \lambda_\eta(k) = (\mathbf{S}^x \mathbf{\Lambda} \mathbf{S}^y)_{kk} \end{array}\right\} k \subset \{1, K\}$$
$$\eta = 1, 2 \qquad x = \frac{2 - \eta}{1 + \eta} \qquad y = 1 - x \qquad (17)$$

We can perform two preliminary operations, respectively the difference and the product between λ and γ entries:

$$\mu_\eta(k) = \lambda_\eta(k) - \gamma_\eta(k) \qquad \Omega_\eta(k) = \lambda_\eta(k)\gamma_\eta(k) \qquad (18)$$

We see that the obtention of μ is very similar to that of $\tilde{\varrho}_\Delta$ in (7). It is now possible to derive the normalization factor ϑ,

$$\vartheta_\eta = \frac{1}{2} \sum_{k=1}^{K} \sum_{\zeta = \gamma, \lambda} \zeta_\eta(k) \qquad (19)$$

From μ we obtain two sets of functions similar to the σ_- and σ_+ ones, $\{\mu_1^-, \mu_1^+\}$ and $\{\mu_2^-, \mu_2^+\}$,

$$\mu_\eta^\pm(k) = \frac{1}{2}\left(\sqrt{\mu_\eta^2(k)} \pm \mu_\eta(k)\right) \qquad (20)$$

and give a first approximation to the $\tilde{\chi}$ index,

$$\tilde{\chi}_\eta^\pm = \sum_{k=1}^{K} \mu_\eta^\pm(k)$$
$$\tilde{\chi}_\eta = \frac{1}{2} \sum_{k=1}^{K} \sum_{\omega = +, -} \mu_\eta^\omega(k) = \frac{1}{2} \sum_{\omega = +, -} \tilde{\chi}_\eta^\omega \qquad (21)$$

From the Ω functions one can deliver a linear algebraic approximation to the ϕ_S approximation:
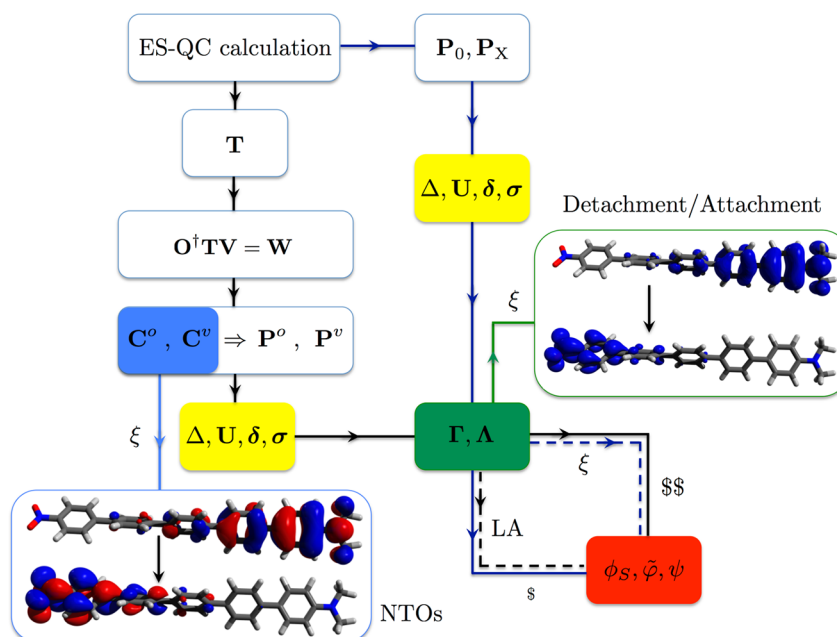
Figure 7. Summary of the different possible derivations of the topological descriptors reported in this article. LA stands for linear algebra, and ξ means that there is a projection in the direct space for visualization and/or numerical integration.

$$\left.\begin{array}{r} \Omega_1(k) \in \mathbb{R}^+ \\ \Omega_2(k) \in \mathbb{R} \end{array}\right\} \Rightarrow \phi_S^\Omega(\eta) =$$

$$\vartheta_\eta^{-1} \sum_{k=1}^K \left[\frac{1}{\eta}\sqrt{\Omega_\eta^\eta(k)} + \left(\frac{\eta-1}{\eta}\right)\Omega_\eta(k) \right]^{1/\eta} \in [0; 1[\tag{22}$$

One can finally perform some simple transformations to obtain $\tilde{\varphi}$, and hence the Φ and ψ descriptors:

$$\tilde{\varphi}_\eta = \vartheta_\eta^{-1}\tilde{\chi}_\eta$$

$$\Phi(\eta) = \tilde{\varphi}_\eta + i\phi_S^\Omega \psi_\eta = 2\pi^{-1}\arctan\left(\frac{\phi_S^\Omega(\eta)}{\tilde{\varphi}_\eta}\right) \tag{23}$$

2.4. Computational Strategy. All the equilibrium geometries reported in the Results section were obtained using the density functional theory (DFT) at the PBE0/6-311G(d,p) level[40−42] with tight convergence criteria. Those geometries are confirmed to be true minima thanks to frequency calculations. All the excited-state calculations were performed using the 6-311++G(2d,p) basis set.[42] For each molecule, six transitions were calculated within the linear response time-dependent DFT framework.[43]

For the illustration of Φ (Figure 3), we computed the second transition of the target compound with the B3LYP xc-functional.[44,45] Acetonitrile solvent effects were accounted for with a self-consistent reaction field, specifically the integral equation formalism of the polarizable continuum model (IEF-PCM).[46−48]

Computation of the family of dyes' (1,4 -nitroaniline derivatives; see Figure 4, below) first transition was performed with the PBE0 xc-functional in acetonitrile.

Finally, validation of the linear algebraic derivation of the indices reported in this article was done by computing the first transition of five families of push–pull dyes (see Figure 5, below) both in vacuum and in acetonitrile. This validation has

been extended with two transition metal complexes,[49] one homoleptic and one heteroleptic (see Figure 6, below), for which there are more than one couple of NTOs bearing the physical information related to the 11th (homoleptic) and 3rd (heteroleptic) transitions. For this purpose, 30 transitions were computed in acetonitrile at the HCTC/6-31+G(d,p)//B3LYP/LANL2DZ{Fe};6-31+G(d,p){C,H,N} level of theory.[44,45,50]

All the calculations were performed with revision B01 of Gaussian 09,[51] and evaluation of the topological descriptors by numerical integration and linear algebraic operations was done using the NANCY_EX 2.0 software suite, which is freely available online.[52]

3. RESULTS

The projection of Φ in the complex plane provides (see Figure 3) a straightforward and elegant way to visualize the locality of the excited state and provides a direct quantitative idea of the ability of the chromophore to delocalize its electron density upon light absorption.

Figure 4 shows that, with the level of theory in use, an increase of the dye's bridge spatial extension (number of subunits ranging from 1 to 5) induces a dramatic decrease of the first excited states locality. This is explicitly evidenced with the obvious variations of θ_S with respect to n in Figure 4.

To validate the linear algebraic derivation of ψ, we see (Figure 5) that there is a significant difference between the accuracy of the first ($\eta = 1$) and second ($\eta = 2$) types of approximations. Indeed, we see that, while the Löwdin-like approach gives ψ_1 values with deviations from the reference ones remaining below 5%, the Mulliken-like approximation for ψ_2 deviates more from the numerical integration entries.

As expected, the linear algebraic approximation's accuracy is basis set-dependent. Indeed, one observes that the lower the ψ value, the better is the match between approximated and reference values. We actually know that, for these families of compounds computed with this level of theory, a low overlap between detachment and attachment densities together with a

high value for the charge-transfer integral, hence a low value for the ψ index, is characteristic of large spacers requiring larger basis sets. This actually means that, considering the high accuracy reported in Figure 5 for the low entries of ψ, the molecular systems with a significant spatial extension are perfectly suited to a linear algebraic assessment of the topological descriptors related to their excited states.

Since this alternative derivation of the charge-transfer quantities was originally introduced to overcome the (sometimes) substantial computational cost of numerical integrations involving high-resolution grids, we can conclude that it is possible to quantitatively assess the locality of excited states of large molecules with linear algebra.

This validation has been extended to iron-based complexes for which the excited state of interest is depicted by more than one couple of NTOs. Figure 6 reports the very close values for ψ obtained by numerical integration and linear algebra. The original (ground/excited states' density matrices-based) and alternative (transition density matrix-based) derivations are shown to deliver identical results.

In summary, and as explicitly reported in Figure 7, the overlap and charge-transfer integrals together with the general ψ index can be equivalently derived from operations performed on ground/excited states' density matrices and transition density matrix, followed by a population analysis or a numerical integration.

4. CONCLUSION

In this article we present a novel strategy to quantitatively probe the charge-transfer ability of a chromophore with quantum chemistry. This approach involves an adequate combination of two photophysical descriptors into a unique index of excited states' topology and can be equivalently derived using natural transition orbitals and ground/excited states' density matrices.

This general quantity, ψ, was further shown to be accurately derived with a cost-effective method involving the contraction of detachment/attachment density matrices with the LCAO basis set overlap matrix, followed by a straightforward population analysis.

Finally, an extensive validation of this alternative strategy was given, and the method was shown to be particularly accurate, and hence suitable for large systems suffering a high computational cost, for the topological descriptors' assessment due to numerical integration.

■ AUTHOR INFORMATION

Corresponding Author

*E-mail: thibaud.etienne@univ-lorraine.fr.

Notes

The authors declare no competing financial interest.

■ REFERENCES

(1) Monari, A.; Assfeld, X.; Beley, M.; Gros, P. C. *J. Phys. Chem. A* **2011**, *115*, 3596−3603.

(2) Dreuw, A.; Head-Gordon, M. *Chem. Rev.* **2005**, *105*, 4009−4037.

(3) Mayer, I. *Chem. Phys. Lett.* **2007**, *443*, 420−425.

(4) Very, T.; Despax, S.; Hébraud, P.; Monari, A.; Assfeld, X. *Phys. Chem. Chem. Phys.* **2012**, *14*, 12496−12504.

(5) Chantzis, A.; Very, T.; Daniel, C.; Monari, A.; Assfeld, X. *Chem. Phys. Lett.* **2013**, *578*, 133−137.

(6) Lachaud, F.; Jeandon, C.; Monari, A.; Assfeld, X.; Beley, M.; Ruppert, R.; Gros, P. C. *Dalton Trans.* **2012**, *41*, 12865−12871.

(7) Chantzis, A.; Very, T.; Monari, A.; Assfeld, X. *J. Chem. Theory Comput.* **2012**, *8*, 1536−1541.

(8) Lachaud, F.; Jeandon, C.; Beley, M.; Ruppert, R.; Gros, P. C.; Monari, A.; Assfeld, X. *J. Phys. Chem. A* **2012**, *116*, 10736−10744.

(9) Monari, A.; Very, T.; Rivail, J.-L.; Assfeld, X. *Comput. Theor. Chem.* **2012**, *990*, 119−125.

(10) Etienne, T.; Michaux, C.; Monari, A.; Assfeld, X.; Perpète, E. A. *Dyes Pigm.* **2014**, *100*, 24−31.

(11) Plasser, F.; Wormit, M.; Dreuw, A. *J. Chem. Phys.* **2014**, *141*, No. 024106.

(12) Plasser, F.; Bäppler, S. A.; Wormit, M.; Dreuw, A. *J. Chem. Phys.* **2014**, *141*, No. 024107.

(13) Bäppler, S. A.; Plasser, F.; Wormit, M.; Dreuw, A. *Phys. Rev. A* **2014**, *90*, No. 052521.

(14) Etienne, T.; Assfeld, X.; Monari, A. *J. Chem. Theory Comput.* **2014**, *10*, 3896−3905.

(15) Etienne, T.; Assfeld, X.; Monari, A. *J. Chem. Theory Comput.* **2014**, *10*, 3906−3914.

(16) Ciofini, I.; le Bahers, T.; Adamo, C.; Odobel, F.; Jacquemin, D. *J. Phys. Chem. C* **2012**, *116*, 11946−11955.

(17) Ciofini, I.; le Bahers, T.; Adamo, C.; Odobel, F.; Jacquemin, D. *J. Phys. Chem. C* **2012**, *116*, 14736−14736.

(18) Guido, C. A.; Cortona, P.; Mennucci, B.; Adamo, C. *J. Chem. Theory Comput.* **2013**, *9*, 3118−3126.

(19) Guido, C. A.; Cortona, P.; Adamo, C. *J. Chem. Phys.* **2014**, *140*, No. 104101.

(20) Le Bahers, T.; Adamo, C.; Ciofini, I. *J. Chem. Theory Comput.* **2011**, *7*, 2498−2506.

(21) Garcia, G.; Adamo, C.; Ciofini, I. *Phys. Chem. Chem. Phys.* **2013**, *15*, 20210−20219.

(22) Jacquemin, D.; Bahers, T. L.; Adamo, C.; Ciofini, I. *Phys. Chem. Chem. Phys.* **2012**, *14*, 5383−5388.

(23) Céron-Carrasco, J. P.; Siard, A.; Jacquemin, D. *Dyes Pigm.* **2013**, *99*, 972−978.

(24) Etienne, T.; Very, T.; Perpète, E. A.; Monari, A.; Assfeld, X. *J. Phys. Chem. B* **2013**, *117*, 4973−4980.

(25) Etienne, T.; Gattuso, H.; Monari, A.; Assfeld, X. *Comp. Theor. Chem.* **2014**, *1040−1041*, 367−372.

(26) Le Bahers, T.; Pauporté, T.; Lainé, P. P.; Labat, F.; Adamo, C.; Ciofini, I. *J. Phys. Chem. Lett.* **2013**, *4*, 1044−1050.

(27) Etienne, T.; Chbibi, L.; Michaux, C.; Assfeld, X.; Monari, A. *Dyes Pigm.* **2014**, *101*, 203−211.

(28) Sharmoukh, W.; Attanzio, A.; Busatto, E.; Etienne, T.; Carli, S.; Monari, A.; Assfeld, X.; Beley, M.; Caramori, S.; Gros, P. C. *RSC Adv.* **2015**, *5*, 4041−4050.

(29) Labat, F.; Le Bahers, T.; Ciofini, I.; Adamo, C. *Acc. Chem. Res.* **2012**, *45*, 1268−1277.

(30) Hagfeldt, A.; Grätzel, M. *Acc. Chem. Res.* **2000**, *33*, 269−277.

(31) Preat, J.; Hagfeldt, A.; Perpète, E. A. *Energy Environ. Sci.* **2011**, *4*, 4537−4549.

(32) Preat, J.; Michaux, C.; Jacquemin, D.; Perpète, E. A. *J. Phys. Chem. C* **2009**, *113*, 16821−16833.

(33) Dedeoglu, B.; Aviyente, V.; Özen, A. S. *J. Phys. Chem. C* **2014**, *118*, 6385−6397.

(34) Dedeoglu, B.; Monari, A.; Etienne, T.; Aviyente, V.; Özen, A. S. *J. Phys. Chem. C* **2014**, *118*, 23946−23953.

(35) Amos, A. T.; Hall, G. G. *Proc. R. Soc. London; Ser. A* **1961**, *263*, 483−493.

(36) Luzanov, A. V.; Sukhorukov, A. A.; Umanskii, V. É. *Theor Exp Chem.* **1976**, *10*, 354−361.

(37) Martin, R. L. *J. Chem. Phys.* **2003**, *118*, 4775−4777.

(38) Batista, E. R., Martin, R. L.Natural transition orbitals. In *Encyclopedia of Computational Chemistry: Quantum Mechanics—Theory and Development*; von Rague Schleyer, P., Allinger, N. L., Clark, T., Gasteiger, J., Kollman, P. A., Schaefer, H. F., Schreiner, P. R., Eds.; John Wiley & Sons Ltd: Chichester, UK, 2004.

(39) Mayer, I. *Chem. Phys. Lett.* **2007**, *437*, 284−286.

(40) Adamo, C.; Barone, V. *J. Chem. Phys.* **1999**, *110*, 6158−6170.

(41) Adamo, C.; Scuseria, G. E.; Barone, V. *J. Chem. Phys.* **1999**, *111*, 2889−2899.

(42) Frisch, M. J.; Pople, J. A.; Binkley, J. S. *J. Chem. Phys.* **1984**, *80*, 3265−3269.

(43) Casida, M. E. *J. Mol. Struct.: THEOCHEM* **2009**, *914*, 3−18.

(44) Becke, A. D. *J. Chem. Phys.* **1993**, *98*, 5648−5652.

(45) Lee, C.; Yang, W.; Parr, R. G. *Phys. Rev. B* **1988**, *37*, 785−789.

(46) Tomasi, J.; Mennucci, B.; Cammi, R. *Chem. Rev.* **2005**, *105*, 2999−3094.

(47) Cancès, E.; Mennucci, B.; Tomasi, J. *J. Chem. Phys.* **1997**, *107*, 3032−3041.

(48) Mennucci, B.; Cancès, E.; Tomasi, J. *J. Phys. Chem. B* **1997**, *101*, 10506−10517.

(49) Duchanois, T.; Etienne, T.; Beley, M.; Assfeld, X.; Perpète, E. A.; Monari, A.; Gros, P. C. *Eur. J. Inorg. Chem.* **2014**, 3747−3753.

(50) Boese, A. D.; Handy, N. C. *J. Chem. Phys.* **2001**, *114*, 5497−5503.

(51) Frisch, M. J., Trucks, G. W., Schlegel, H. B., Scuseria, G. E., Robb, M. A., Cheeseman, J. R., Scalmani, G., Barone, V., Mennucci, B., Petersson, G. A., Nakatsuji, H., Caricato, M., Li, X., Hratchian, H. P., Izmaylov, A. F., Bloino, J., Zheng, G., Sonnenberg, J. L., Hada, M., Ehara, M., Toyota, K., Fukuda, R., Hasegawa, J., Ishida, M., Nakajima, T., Honda, Y., Kitao, O., Nakai, H., Vreven, T., Montgomery, J. A., Peralta, J. E., Ogliaro, F., Bearpark, M., Heyd, J. J., Brothers, E., Kudin, K. N., Staroverov, V. N., Keith, T., Kobayashi, R., Normand, J., Raghavachari, K., Rendell, A., Burant, J. C., Iyengar, S. S., Tomasi, J., Cossi, M., Rega, N., Millam, J. M., Klene, M., Knox, J. E., Cross, J. B., Bakken, V., Adamo, C., Jaramillo, J., Gomperts, R., Stratmann, R. E., Yazyev, O., Austin, A. J., Cammi, R., Pomelli, C., Ochterski, J. W., Martin, R. L., Morokuma, K., Zakrzewski, V. G., Voth, G. A., Salvador, P., Dannenberg, J. J., Dapprich, S., Daniels, A. D., Farkas, O., Foresman, J. B., Ortiz, J. V., Cioslowski, J., Fox, D. J. *Gaussian 09*, revision B.01; Gaussian, Inc.: Wallingford, CT, 2010.

(52) http://nancyex.sourceforge.net (accessed February 5, 2015).